A 6-Components Mechanistic Model of Cutting Actions in Milling

Maël Jeulin (mael.jeulin@u-bordeaux.fr)
Univ. Bordeaux https://orcid.org/0000-0003-3393-6166
Olivier Cahuc
Univ. Bordeaux
Philippe Darnis
Univ. Bordeaux
Raynald Laheurte
Univ. Bordeaux

Research Article

Keywords: 3-dimensional milling, Energy balance, Cutting moment, Cutting model, 3-dimensional chip section

Posted Date: November 30th, 2021

DOI: https://doi.org/10.21203/rs.3.rs-1114156/v1

A 6-Components Mechanistic Model of Cutting Actions in Milling

Maël Jeulin[1*], Olivier Cahuc[1†], Philippe Darnis[1†] and Raynald Laheurte[1†]

[1*]Univ. Bordeaux, I2M UMR 5295, 351 cours de la Libération, Talence, F-33400, France.

*Corresponding author(s). E-mail(s): mael.jeulin@u-bordeaux.fr;
Contributing authors: olivier.cahuc@u-bordeaux.fr;
philippe.darnis@u-bordeaux.fr; raynald.laheurte@u-bordeaux.fr;
†These authors contributed equally to this work.

Abstract

Most of the cutting models developed in the literature attest only to the presence of cutting forces in the balance of mechanical actions resulting from cutting. However, several studies have highlighted the presence of cutting moments during machining, and particularly 3D cutting in milling. The objective of this paper is to characterise phenomena associated with cutting moments by performing experimental mechanistic modelling in 3D cutting. For this purpose, several modelling factors will be investigated, such as the 3D cutting reference frame, the undeformed chip section, the cutting parameters, the cutting zone, etc. The predictive model of this study proves to be relatively efficient for an experimental model and allows a global prediction of cutting moments in milling. Furthermore, beyond the aspect of stress fields in the workpiece caused by cutting moments, this paper gives perspectives from an energetic point of view for which the share of moments in the energy balance could be substantial for monobloc tools.

Keywords: 3-dimensional milling, Energy balance, Cutting moment, Cutting model, 3-dimensional chip section

Nomenclature

V_c	Cutting speed (m/min)
V_f	Feed velocity (m/min)
f	Feed rate (mm/tr)
a_p	Depth of cut (mm)
κ_r	Tool cutting edge angle (°)
γ_0	Rake angle (°)
λ_s	Cutting edge inclination (°)
C_c	Tool centre position
C_e	Cutting edge position
$\mathcal{R}_0$ $(\mathrm{O}, \vec{x_0}, \vec{y_0}, \vec{z_0})$	Fixed reference of the sensor applied to the measure origin O
$\mathcal{R}_t$ $(C_e, \vec{e_r}, \vec{e_\theta}, \vec{z_0})$	Local reference mark of the lathe applied to the cutting edge position C_e
$\mathcal{R}_{cp}$ $(P, \overrightarrow{e_{r_{cp}}}, \overrightarrow{e_{\theta_{cp}}}, \overrightarrow{z_{cp}})$	Local cutting plane reference applied to the application point of the cutting P
θ	Angular position of the cutting edge (°)
$\vec{\omega}_{\text{tool/workpiece}}$ $(\vec{\omega})$	Angular speed field of the tool relative to the workpiece
$\vec{V}_{P,\text{tool/workpiece}}$ $\left(\vec{V}_P\right)$	Velocity field of the tool relative to the workpiece at point P
$\vec{\mathcal{F}}_{\text{workpiece}\to\text{tool}}$	Force field of the workpiece on the tool
$\vec{\mathcal{M}}_{P,\text{workpiece}\to\text{tool}}$	Moment field of the workpiece on the tool at point P
Y_c	y_0-axis coordinate of the tool center (mm)
S_{chip}	Chip section (mm^2)
Δe_r	Instantaneous radial feed rate (mm)
Δf	Instantaneous axial feed rate (mm)
$C_{*,i}(\theta_j)$	Discretised position in round of cut i, at discretised angular position θ_j
ω_z	Tool angular speed (rad/s)
K_{m2}, K_{m1}	Polynomial cutting moment model parameters

Introduction

Machining processes modelling constitute a substantial amount of work in the mechanical engineering literature. Products quality, processes sustainability, new manufacturing processes or even digital manufacturing are the main issues of this field. In order to improve the sustainability of machining processes, this paper focus on a mechanistic model of the cutting in milling which allow a complete and accurate energy balance.

Actually, mechanical cutting models are the essentials of energy consumption prediction during milling. Correctly predicting this energy balance makes it possible to anticipate manufacturing costs and even its environmental impact. Quantities of cutting models were developed in the literature which consider exclusively cutting forces as source of energy consumptions. However, the I2M laboratory highlighted that a large amount of energy losses were not quantified by considering only the cutting forces. Indeed, the contribution of the cutting moments constitutes a significant part of the energy balance in machining, especially at high cutting speed [1]. Moreover, the other issue is the characterisation of the mechanical behaviour of the material subjected to cutting stresses (residual stresses) and the cutting moments contribute to residual stresses of the workpiece.

This paper describes an experimental model integrating the cutting moments for a specific configuration and gives tools to predict these coefficients in 3D cutting. In the first section, the 3D cutting model considered is defined. Then, the experimental protocol and the material used are described. Finally, the last paragraph is devoted to the results and their analysis, with the proposal of a mechanistic model of cutting moments.

1 Milling cutting model

1.1 Definition of 3D cutting parameters

In milling, the tools used for most operations have a particular geometry with a 3D orientation of the cutting face. The tools can be one-piece tools or insert tools which were used for the study.

The main geometric and kinematic cutting parameters (defined in Figure 1) are:

- the cutting speed $\mathbf{V}_c$
- the feed velocity $\mathbf{V}_f$ / the feed rate $\mathbf{f}$
- the depth of cut $\mathbf{a}_p$
- the tool cutting edge angle κ_r
- the rake angle γ_0
- the cutting edge inclination λ_s

The 3D geometrical parameters of the tooth orientation are defined in Figure 1 with respect to the tooth's rotational reference ($\vec{e_r}$, $\vec{e_\theta}$, $\vec{z_0}$). Special cases of the 3D cutting such as the orthogonal or the oblique cutting are to be notified as they are the most studied cases for the simplicity of the associated cutting process phenomenology. Figure 1 also shows the special case of the orthogonal cutting ($\lambda_s = 0°$, $\kappa_r = 90°$, any γ_0) for a milling operation.

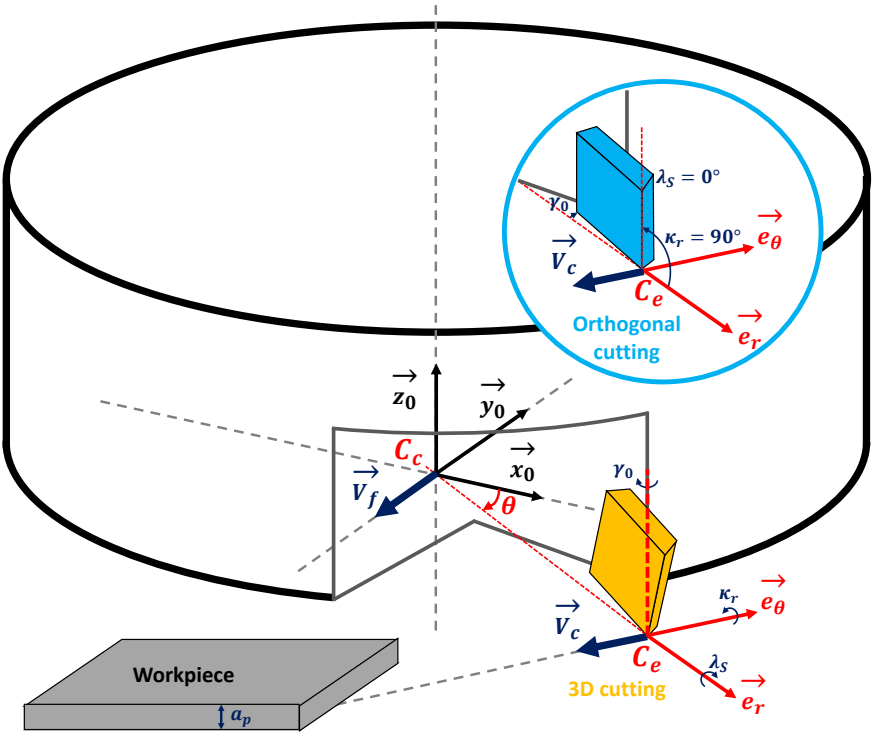

Fig. 1 Definition of geometric and kinematic cutting parameters

1.2 Cutting process phenomenology

Cutting is a process that removes a chip from a workpiece to form one or more surfaces. For this purpose, the cutting can be of different orders because of the complexity of desired geometries. Yousfi [2] has theoretically demonstrated the complexity of the cutting phenomena occurring in 3D cutting, in particular the complexity of the kinematic fields linked to the associated tool geometry. This has repercussions on the shape of the chip, which differs according to the type of cutting (Figure 2). Indeed, 3D cutting generates 3D cutting mechanical actions which cause 3D deformation of the chip, at the origin of the associated complex cutting phenomena.

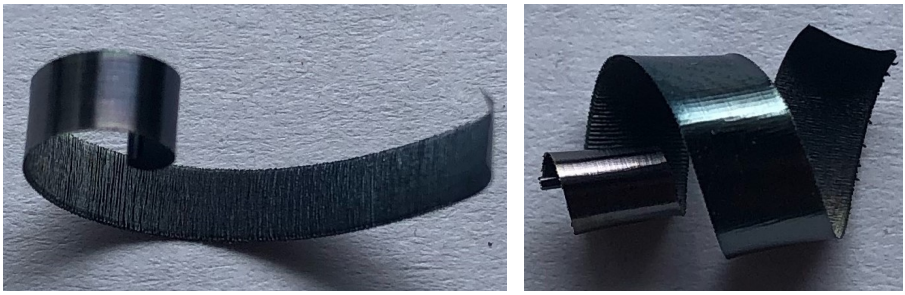

(a) (b)

Fig. 2 (a) Chip in orthogonal cutting; (b) Chip in 3D cutting

Quantities of tests in the literature have therefore been carried out in orthogonal cutting to establish simple and usable cutting models, generally related to the chip section. These models mainly highlight the cutting forces which are the most studied properties in the literature. For tools with inserts, most papers are restricted to the geometrical and kinematic parameters of orthogonal cutting (V_c, f, a_p, γ_0), nevertheless studies have been carried out on the influence of material parameters for example (hardness, thermal conductivity, mechanical strength) [3–5].

However, basic orthogonal cutting models that have only developed the importance of cutting forces linearly dependent on the chip section, present significant errors in their modelled energy consumption [1]. This is why the development of cutting moments theory was a major step towards completing the cutting energy balance. This is the case of Albert [6] who started to highlight the cutting moment phenomenology with orthogonal cutting tests in milling. The objective of this paper is therefore to characterise the behaviour of 3D cutting, mainly that of the cutting moments, based on the work on cutting forces carried out in the literature.

For this purpose, the cutting moments phenomena must be studied and analysed, starting with the expression point starting where the modeling is most relevant. Indeed, the value of the cutting moments is different depending on the application point, so it is essential to establish a significant point of application P where to express the cutting moments. The theoretical application point of the cutting P should be at the barycentre of the tool force density on the workpiece. In fact this point is complex to determine experimentally because the measurement of mechanical actions is the force vector and not the measurement of the cutting force density. The application point P is assumed to be located in the cutting zone, as this is the most physically significant area with the cutting force density concentrated on it.

However, the theoretical application point of the cutting P is a secondary element for the energy balance and is only a calculation point for the mechanical power. Indeed, the mechanical power (which by hypothesis represents the consumed machining power) does not depend on the application point nor on the expression reference of the mechanical and kinematic components. In the context of machining, the hypothesis of undeformable solids is used because the mechanical actions components of the energy balance are measured and global. The internal mechanical power developed by machining, calculated at the point P, is then described:

$$\begin{aligned} \mathscr{P}_{\text{tool} \leftrightarrow \text{workpiece}} = \quad & \vec{\mathcal{F}}_{\text{workpiece} \rightarrow \text{tool}} \cdot \vec{V}_{P,\, \text{tool/workpiece}} \\ & + \vec{\mathcal{M}}_{P,\, \text{workpiece} \rightarrow \text{tool}} \cdot \vec{\omega}_{\text{tool/workpiece}} \end{aligned} \tag{1}$$

To demonstrate the presence of pure cutting moments, it is sufficient that the proportion of power related to moments in the energy balance is non-null. Furthermore, the central axis theory can then be applied to calculate the value of these pure cutting moments. Several studies have identified the main sources of cutting moment creation as follows:

- Pure torques related to intra-grain spin at the microstructural scale of the material, caused by high cutting stresses [7].
- Torques induced by the 3D geometric and kinematic cutting phenomenology [8].
- Frictional moments generated by intense tribological phenomena at the tool/workpiece/chip interface with specific friction conditions (high pressure and temperature, strain hardening, variable chip section, etc.), studied mainly in the literature on cutting forces [9], but also applicable to cutting moments.

1.3 Definition of the chip section

The accurate identification of the chip section is an important issue for the modelling of cutting actions as it is the basis of main experimental cutting models. To begin with, for a straight tool path, the theoretical trajectory described by the tool tip is trochoidal because it is composed of a circular motion related to the tool rotation as well as an axial feed rate to follow the imposed path (Figure 3).

The most common model of the chip section is the normalized orthogonal chip section defined in the plane orthogonal to the cutting speed $\vec{V}_c$ [6, 10]. It is defined as follows:

$$S_{\text{chip}} = \Delta e_r \times a_p \tag{2}$$

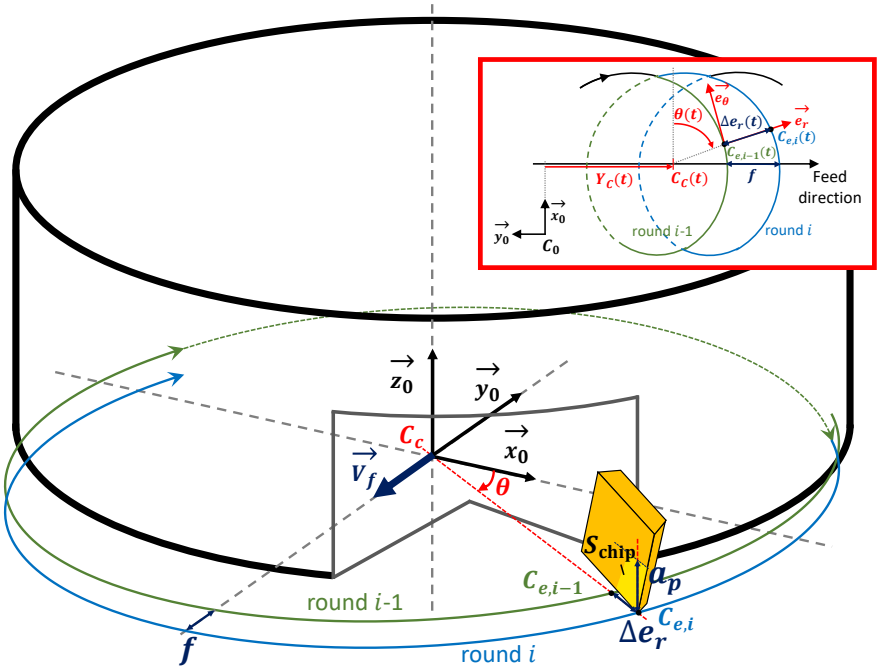

Fig. 3 Definition of the trochoidal tool path $C_{e,i}(t)$

This section actually corresponds to the chip section not yet deformed by the cutting, before the tool cuts the material. This is why the instantaneous radial feed rate Δe_r must be accurately modelled with an automated algorithm for each discretised cutting point $C_{e,i}$.

The calculation of Δe_r is supported by an explanatory diagram showing the key elements of the calculation (Figure 4) with the associated algorithm defined in Appendix A. One of them is the instantaneous axial feed rate Δf, which takes into account the deceleration of the tool from its initial trajectory due to the high cutting forces. Indeed, experimental observations during the cutting process indicate a non-negligible deceleration that causes the instantaneous radial feed rate Δe_r vary by up to 10% according to the various tests conducted, submitted to the section 2.2.

The actual undeformed chip section associated with the cutting face can be defined as the orthogonal projection along $\vec{e_\theta}$ of the normalized orthogonal chip section on the 3D insert (Figure 5). The value of the chip section then becomes with $\gamma_0 = 0°$:

$$S_{\text{chip 3D}} = (\Delta e_r \times a_p - S_{\text{residual}}) \,/\, \cos\lambda_s \tag{3}$$

This chip section is more representative for characterising the phenomena studied because they occur at the cutting face, at the tool/workpiece interface.

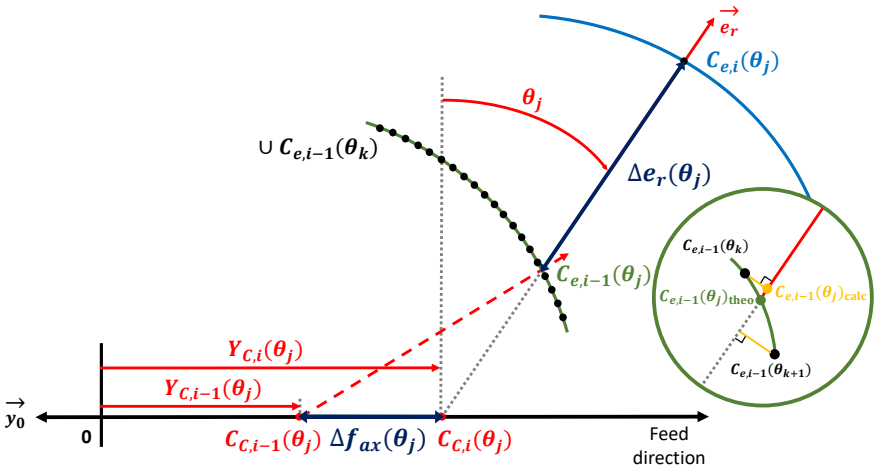

Fig. 4 Algorithmic calculation of the instantaneous radial feed rate Δe_r

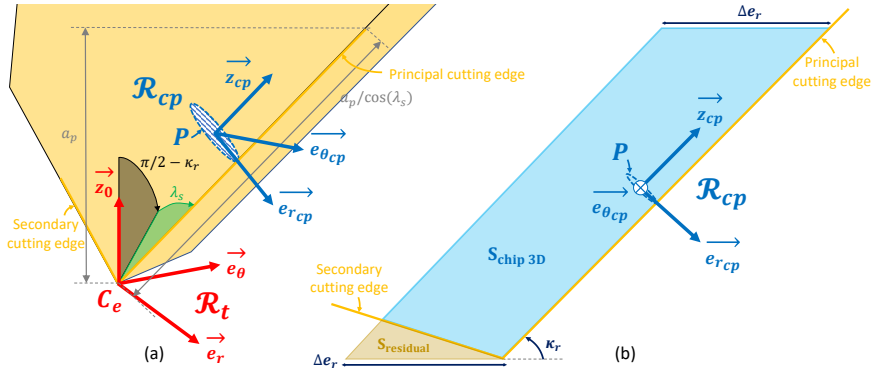

Fig. 5 Definition of the 3D undeformed chip section associated to the reference $\mathcal{R}_{cp}$ ($\gamma_0 = 0°$) : (a) 3D view, (b) 2D cutting plan view

1.4 3D kinematic fields

As each machine position $\overrightarrow{Pos_P}(X_P, Y_P, Z_P)$ at point P is discretised at regular time intervals Δt, the instantaneous local speed $\overrightarrow{V_P}$ is defined as follows:

$$\overrightarrow{V_P} = \frac{\overrightarrow{\Delta Pos_P}}{\Delta t} \tag{4}$$

This velocity can be applied to the local basis ($C_{e,i}$, $\vec{e_r}$, $\vec{e_\theta}$, $\vec{z_0}$) turned at the discretised θ_j angle:

$$\begin{cases} V_{C_{e,i},e_r} = \left(\Delta X_{C_{e,i}} \cos\theta_j + \Delta Y_{C_{e,i}} \sin\theta_j\right)/\Delta t \\ V_{C_{e,i},e_\theta} = \left(\Delta Y_{C_{e,i}} \cos\theta_j - \Delta X_{C_{e,i}} \sin\theta_j\right)/\Delta t \\ V_{C_{e,i},z_0} = \Delta Z_{C_{e,i}}/\Delta t \end{cases}$$

Intrinsic variations of the $(X_{C_e}, Y_{C_e}, Z_{C_e})$ components from the nominal trochoidal path may correspond to the deceleration of the tool demonstrated by the variation of the instantaneous axial feed rate Δf.

The tool rotational speed $\omega_{z,j}$ is defined such that it accounts for the deceleration of the tool during the cutting process:

$$\omega_{z,j} = \Delta\,\theta_{j,j-1}/\Delta t \tag{5}$$

A cutting plane reference $\mathcal{R}_{cp}$ can be defined from the geometrical rotations of the insert. Indeed, this reference $\mathcal{R}_{cp}$ characterises the cutting face (Figure 5) which is more representative of the cutting process than the normalized orthogonal face $(\vec{e_r}, \vec{z_0})$.

2 Experimental approach

An experimental set-up was carried out to develop the experimental mechanistic model of the cutting phenomenon wanted.

2.1 Material used

To perform the milling tests, a 3-axis **Rosilio** C850 machine-tool was used (Table 1). The experimental setup is shown in Figure 6. It consists of a **Kistler** 9129AA 6-component high dynamic force dynamometer (Table 2) directly fixed on the machine-tool table. Subsequently, this stage supports the AISI 4142 (42CrMo4) alloy steel samples chosen to characterise the tests for which the composition is described Table 3.

Max spindle power (kW)	Max spindle speed (rpm)	Axis strokes (mm)	Feed rates (m/min)	Digital control
20	15000	X: 800 Y: 510 Z: 610	X: 20 Y: 20 Z: 24	**Heidenhain** ITNC 530

Table 1 Characteristics of the **Rosilio** C850

Number of sensors	Max permitted measuring range forces (kN)	Max of permitted measuring range of moments ($N.m$)
4	-10 ... 10	-500 ... 500

Table 2 Characteristics of the **Kistler** dynamometer

(%)	C	Si	Mn	P	S	Cr	Mo
from	0.38	-	0.60	-	-	0.90	0.15
to	0.45	0.40	0.90	0.25	0.35	1.20	0.30

Table 3 Chemical composition of the AISI 4142 (42CrMo4) alloy steel

Fig. 6 Experimental setup for milling tests

To recover the data from the dynamometer and the machine-tool, a post-processing software **DeweSoft** is used. It allows the recovery of the force and moment components developed during machining as well as the machine positions. The acquisition frequency is set at 50 kHz to characterise passes of a few hundredths of a second, varying according to the imposed cutting speed.

The tool used for the cutting tests is an **ISCAR** HOF D040-04-22-R06 milling cutter having a single tooth with an **ISCAR** OEMW 060405-AETN IC808 octagonal carbide insert with Aluminium-Titanium-Nitride (AlTiN) coating (Figure 6) and measured orientation geometry parameters $\gamma_0 = 0°$, $\kappa_r = 38°$, $\lambda_s = 15°$.

In order to get usable results, filtering of the data is necessary to eliminate the noise caused by the very high dynamics of the measurement system. As the noise appears at high frequency, a low-pass filter is used for each test to recover only the frequency around the number of rounds of cut per second, which is at a rather low frequency as the cutting speeds are reasonable. This frequency corresponds to the amplitude of the periodic phenomena of the cutting, thus the relevant cutting mechanical actions.

2.2 Experimental protocol

Numerous orthogonal cutting tests carried out by Albert [6] have enabled initial interpretations of the cutting moment process phenomenology. An interesting result is the influence of the orthogonal parameters V_c, f, a_p on the preponderance of cutting moments. Indeed, Albert [11] demonstrated with the results of his design of experiments, an independence of the cutting parameters (negligible interaction between the parameters) on the value of cutting moments. This assumption of cutting parameter independence is considered for the design of experiments of the milling tests.

The primary objective of the tests is to characterise the cutting moments in the cutting zone and the secondary one is to verify the influence of the cutting parameters V_c, f, a_p on the value of these cutting moments. For this purpose, a reference test (RT) with $V_c = 160\,\text{m/min}$, $f = 0.2\,\text{mm/tooth}$, $a_p = 1.7\,\text{mm}$ is carried out, followed by a design of experiments with the variation of the parameters on 2 levels compared to the reference test. The design of experiments carried out is described in table 4.

N° tests	V_c (m/min)	f (mm/tooth)	a_p (mm)
1 (RT)	160	0.2	1.7
2	80	0.2	1.7
3	240	0.2	1.7
4	160	0.15	1.7
5	160	0.25	1.7
6	160	0.2	1
7	160	0.2	2.4

Table 4 Milling design of experiments

3 Results of cutting moment identification

The test that will illustrate this section is the reference one with parameters $Vc = 160\,\text{m/min}$, $f = 0.2\,\text{mm}$, $ap = 1.7\,\text{mm}$.

3.1 Experimental results and verifications

The resulting pure moments applied to the cutting points P in the cutting plane reference frame $\mathcal{R}_{cp}$ are represented by θ in Figure 7. The existence of the 3D moments highlighted in Figure 7 is indicative of the complexity of the cutting phenomena.

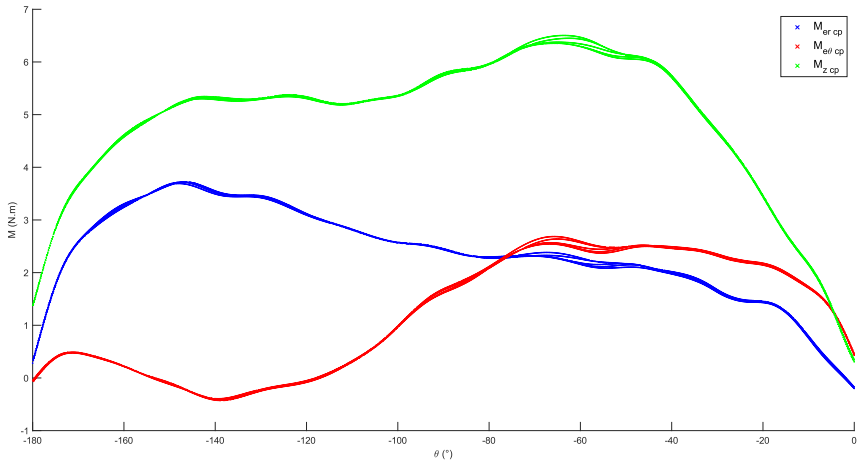

Fig. 7 3D cutting moments at points P in $\mathcal{R}_{cp}$

The positioning of the application point of the cutting P can be estimated experimentally from a minimisation criterion of the cutting moments at the tool/workpiece interface, as the experimentally determined central axis is remote from the cutting zone and therefore has no physical significance. Indeed, the points resulting from this criterion are those which minimise the contribution of the forces to the amplitude of the cutting moments in the cutting zone. The positions of the points P in the cutting plane reference $\mathcal{R}_{cp}$ for each disretised angular position θ are represented in Figure 8. Actually, the points P are located in the index position where the associated minimisation criterion of the cutting moments $\min \left\| \overrightarrow{\mathcal{M}_{\text{mesh}}} \right\|$ is verified.

The position of the points P is close to the principal cutting edge, where the density of the cutting forces is the highest (separation edge of the material), and also on the average line of the chip section, which reflects the homogeneity of the cutting pressures along the direction of the cutting edge $\overrightarrow{z_{cp}}$. This is why the points P at the principal cutting edge and on the average line of the chip section were accepted to model the cutting moments (P characteristic point of the model on the figure 8). The associated leverage for the positioning error of the chosen point P related to the theoretical points P is minor and it is more convenient to have a fixed application point in the cutting zone than a distribution of points P.

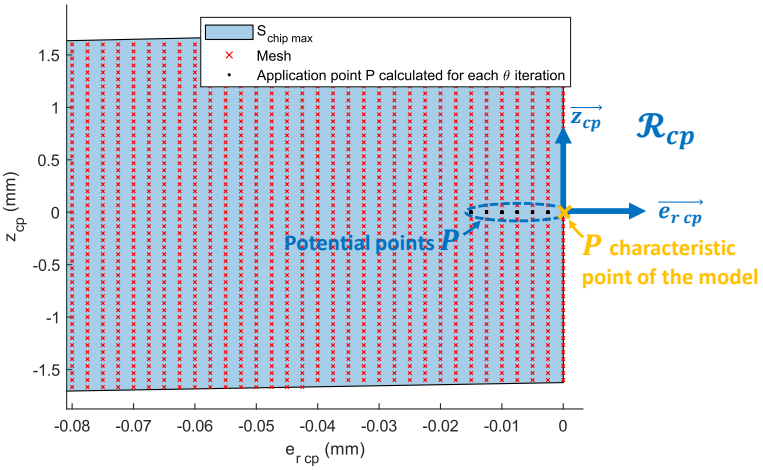

Fig. 8 Positioning of the application points of the cutting P in $\mathcal{R}_{cp}$

3.2 Confirmation of the existence of pure cutting moments

The cutting moments characterised previously could theoretically result from leverage associated with the cutting forces with zero resultant moments expressed at the central axis. To ensure the veracity of the observed phenomenon, the cutting moments at the central axis are represented in Figure 9. The presence of non-negligible moments indicates the relevance of the observed phenomenon. In addition, the cutting energy balance is described in Figure 10 and highlights the importance of the cutting moments in the energy balance with an average relative error of 4% without considering the cutting moments and up to 120 W maximum absolute error, for the reference test. It is noteworthy that cutting moments consume energy during climb cutting and conversely will tend to reduces the energy consumption of the process during conventional cutting. All these elements demonstrate the complex phenomena of cutting moments occurring during milling.

3.3 Identification of specific cutting moment

Most of the work in the literature on the cutting forces modelling has resulted in a linear modelling of the cutting forces as a function of the chip section with the introduction of the specific cutting pressures, introduced firstly by Martellotti [12]. The objective of the paper is to verify whether such kind of models are applicable to cutting moments, especially when they occur strongly in 3D cutting. The following modellings are carried out on the mechanical actions expressed in a reference frame such that their dimension is uni-axial (which amounts to taking the norm of the force field $\vec{\mathcal{F}}$ or of the moment field $\vec{\mathcal{M}}$) in order to set up a global and simple model that does not require an expression reference frame.

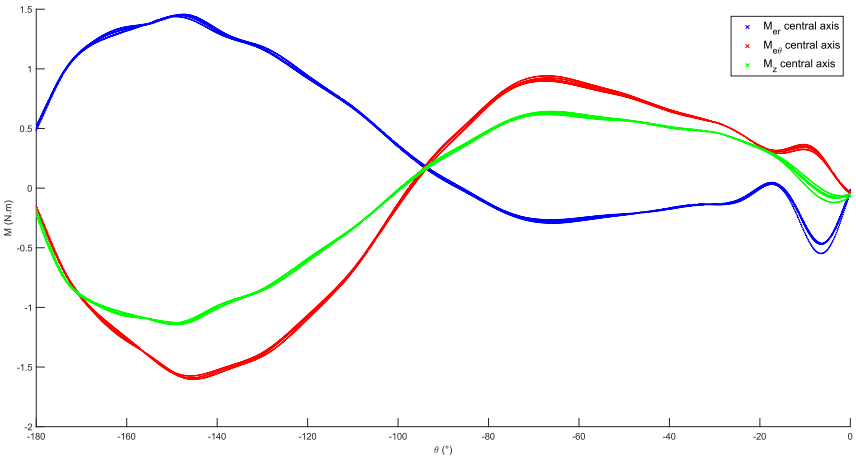

Fig. 9 Pure cutting moments expressed at the central axis in $\mathcal{R}_t$

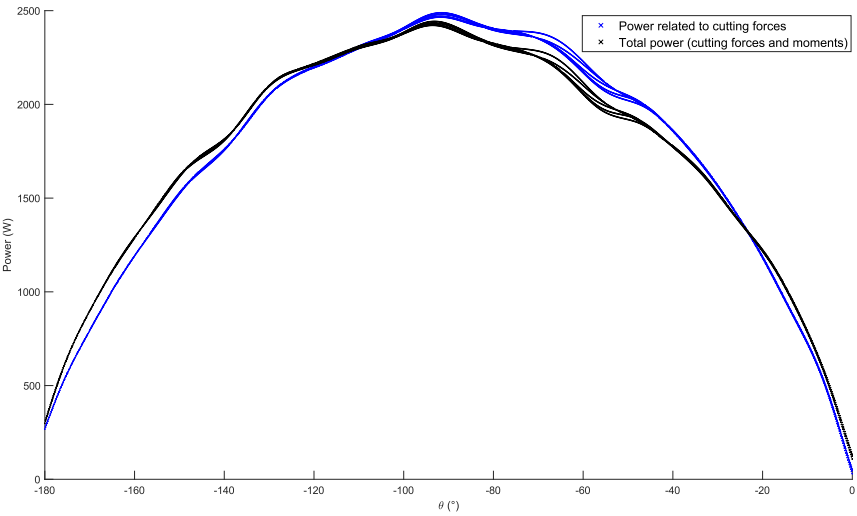

Fig. 10 Power consumed during milling

The first step is to verify whether a linear model as a function of the chip section can correspond to the cutting force profile. Figure 11 shows a linear model, as a function of the chip cross-section, fitting the cutting forces in stable cutting ($\theta \in [-160;\ -20]$). These results satisfy the cutting force models proposed in the literature.

As for the cutting moments, a 2-order polynomial model is proposed, with 2 model coefficients K_{m2} $\left[\text{N.m.mm}^{-4}\right]$ and K_{m1} $\left[\text{N.m.mm}^{-2}\right]$:

$$\mathcal{M}_{P,\,\text{norm}} = \left\|\vec{\mathcal{M}}_P\right\| = K_{m2} \times S^2_{\text{chip 3D}} + K_{m1} \times S_{\text{chip 3D}} \tag{6}$$

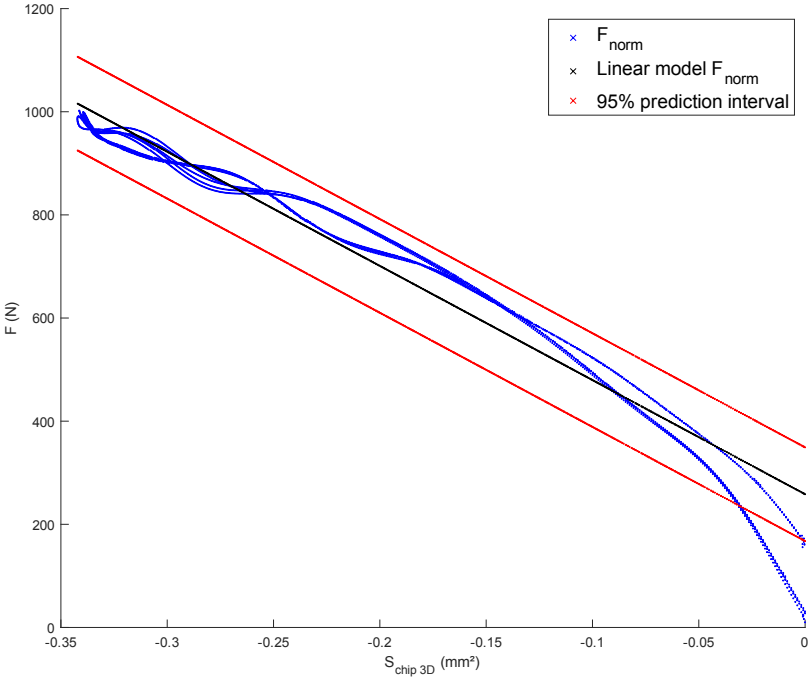

Fig. 11 Linear model of cutting forces by $S_{\text{chip 3D}}$

The result of these models as a function of chip section and angular position θ are shown respectively in Figures 12 and 13. This is the best compromise between modelling difficulty and prediction quality. Indeed, a 5-order mechanistic model based on theta angular position would allow to perfectly fit the cutting moments, however this model would have no physical meaning (modelling by angular position θ) and would be difficult to identify from a model prediction perspective. The chosen model allows for a relatively low Root Mean Square Error (RMSE) of 0.5 N.m while still having a physical meaning (modelling by chip section). Furthermore, the modelling of the cutting moments according to the chip section by a polynomial model reaches its model accuracy limit already at order 2, with a maximal coefficient of determination R^2 of 87%.

3.4 Cutting parameter-based modelling

From the tests conducted, conclusions can be drawn on the influence of the parameters V_c, f, a_p on the value of the model coefficients K_{m1} and K_{m2}. Indeed, the influence of the parameter V_c turns out to be practically null on the two model parameters (within the limit of the cutting speed values supported by the insert used), with non-significant variations of the results compared to the variance analysis. Nevertheless, the influence of the parameters f and a_p shows a priori a linear decreasing trend in the coefficients K_{m1} and K_{m2} with

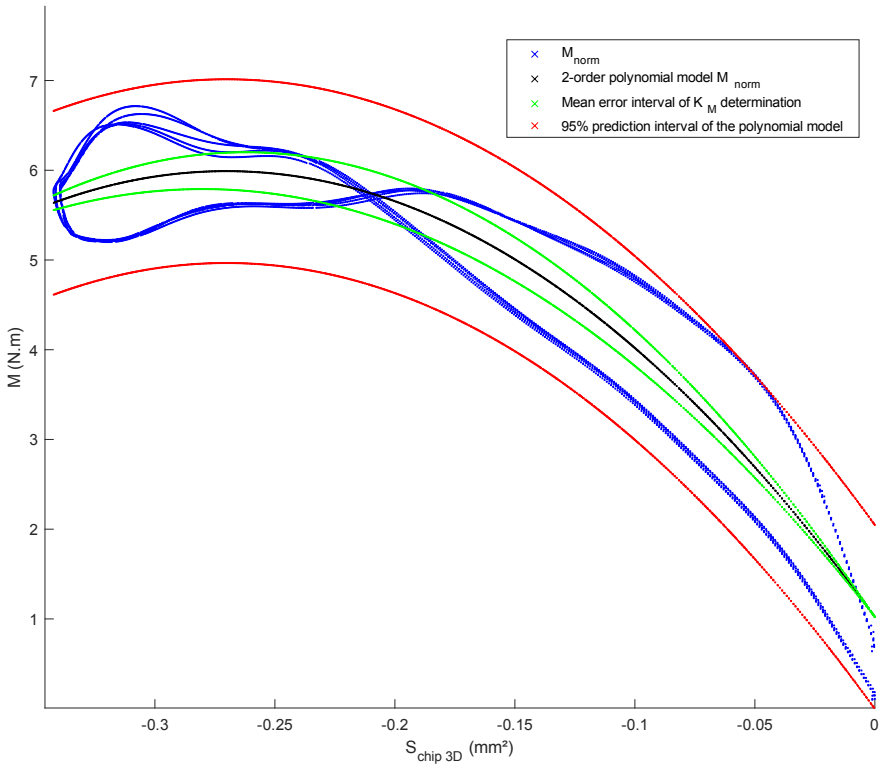

Fig. 12 2-order polynomial model of cutting moments at points P by $S_{\text{chip 3D}}$

significant variations depending on the value of these parameters. As a result, a multilinear model is proposed in the validity zone of the cutting parameters, in order to initiate a prediction approach:

$$\begin{cases} K_{m2} = A_{20} + A_{21} \times f + A_{22} \times a_p \\ K_{m1} = A_{10} + A_{11} \times f + A_{12} \times a_p \end{cases}, A \in \mathbb{R} \tag{7}$$

The linear plan to verify the validity of the model proposed is described in Figure 14. The few tests proposed do not allow us to validate this multilinear model properly, but it does allow to verify that the expected trend is apparently correct. Indeed, the RMSE of K_{m2} is evaluated to 7.3 N.m.mm^{-4} while that of K_{m1} is 2.7 N.m.mm^{-2}. To provide an overview of the accuracy of the model, Figure 12 highlights the average efficiency of the predicted moments on the same model by shifting the coefficients K_{m1} and K_{m2} by the average value of the error calculated RMSE:

$$\begin{aligned} \mathcal{M}_{\text{average predicted}} = &(K_{m2} \pm \text{RMSE}_{K_{m2}}) \times S^2_{\text{chip 3D}} \\ &+ (K_{m1} \pm \text{RMSE}_{K_{m1}}) \times S_{\text{chip 3D}} \end{aligned} \tag{8}$$

These moments are an indicator of the adequacy of the proposed multilinear plan to recover $\mathcal{M}_{P,\,\mathrm{norm}}$. The maximum error associated with the predicted cutting moments is evaluated to 4%.

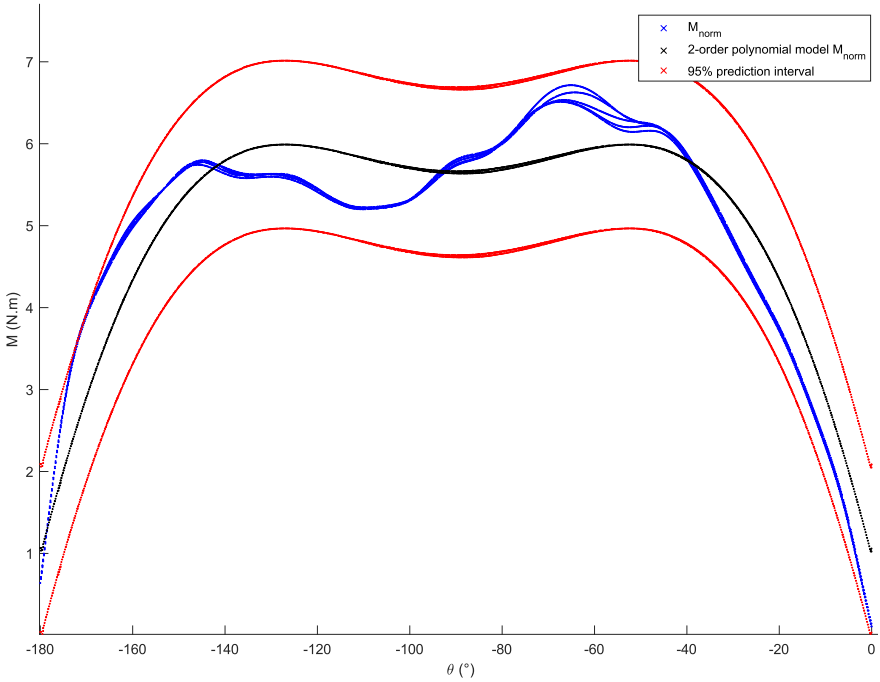

Fig. 13 Verification of the cutting moments model according to θ

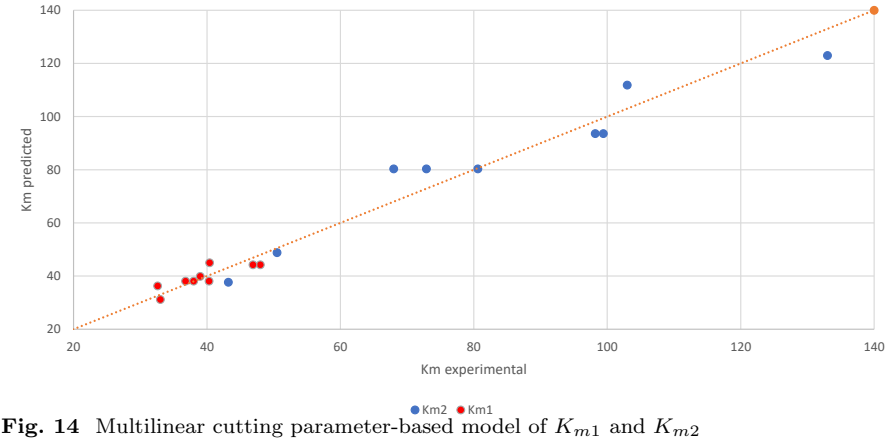

Fig. 14 Multilinear cutting parameter-based model of K_{m1} and K_{m2}

Conclusion

The results proposed in this paper highlight a complex phenomenon of cutting moments during milling. These moments in the cutting zone have a non-negligible impact. The moments generate important mechanical actions on the workpiece that have not yet been qualified, and have an influence on the stresses to which the workpiece is subjected. This could cause alterations in the mechanical properties of the part (deformations of surface quality, material health, etc.) and generate high residual stresses. The simple and physically meaningful model proposed to characterise these moments in the cutting zone shows a relatively large error but which is still acceptable for an experimental model. However, this model can be enriched to reduce the associated error, particularly with others machining configurations.

The perspectives associated with cutting moments are promising because the energy impact (favourably or unfavourably depending on conventional or climb machining) is non-negligible for the tests performed, while the ratio of cutting speed V_c to tool rotation speed ω_z is high. For the same cutting speed V_c with a much smaller tool radius, the tool rotation speed ω_z could increase significantly compared to the cutting speed V_c, and generate a significant part of the energy balance in favour of the cutting moments. As an indication, with a cutting moment profile equivalent to the tests conducted and a ω_z of 2000 rad/s, the share of cutting moments in the energy balance could reach on about 40%.

The future work to be carried out to refine the model and better characterise the phenomena associated with cutting moments consists of:

- Realization of different design of experiments to refine, enrich and validate the proposed mechanistic model
- Use of monobloc tools (small tool radius) in order to see the energetic influence of cutting moments for this type of tool
- Work on the repercussions of cutting moments on the mechanical properties of the workpiece, such as roughness, surface, hardness, residual stresses, ...

Appendix A Algorithm of Δe_r calculation

Algorithm 1 Calculate Δe_r

Require: $\boldsymbol{N_\theta}$, average number of discretised points C_c per round of cut i

$\boldsymbol{N_{cn}}$, arbitrary closest neighbour search factor

Ensure: $\boldsymbol{\Delta f}$, instantaneous axial feed rate

$\Delta f \leftarrow Y_{C,i}(\theta_j) - Y_{C,i-1}(\theta_j)$

Ensure: $\boldsymbol{\Delta e_r}$, instantaneous radial feed rate

for $j = 1 : \sum_{i=2}^{end} \theta_j$ **do**

cns, closest neighbour search set points

cns $\leftarrow (j - N_{cn} - N_\theta) : (j + N_{cn} - N_\theta)$

Calculation of the coefficients of the Cartesian equation of the line $(C_{e,i}(\theta_j)C_{c,i}(\theta_j))$

Calculation of the minimum Euclidean distance between the points $C_{e,i-1}(\theta_{\text{cns}})$ and the line $(C_{e,i}(\theta_j)C_{c,i}(\theta_j))$

$\rightarrow$ **min** index

Projection of the point $C_{e,i-1}(\theta_{\text{min}})$ on the line $(C_{e,i}(\theta_j)C_{c,i}(\theta_j))$

$\rightarrow C_{e,i-1}(\theta_j)_{\text{calc}}$

Calculation of the Euclidean distance between $C_{e,i-1}(\theta_j)_{\text{calc}}$ and $C_{e,i}(\theta_j)$

$\rightarrow \Delta e_r$

end for

References

[1] Cahuc, O., Darnis, P., Gérard, A., Battaglia, J.-L.: Experimental and Analytical Balance Sheet in Turning Applications. Int J Adv Manuf Technol **18**(9), 648–656 (2001). https://doi.org/10.1007/s001700170025

[2] Yousfi, W.: Modélisation thermomécanique 3D en fraisage. phdthesis, Université de Bordeaux (December 2015). https://tel.archives-ouvertes.fr/tel-01263888

[3] Chinchanikar, S., Choudhury, S.K.: Effect of work material hardness and cutting parameters on performance of coated carbide tool when turning hardened steel: An optimization approach. Measurement **46**(4), 1572–1584 (2013). https://doi.org/10.1016/j.measurement.2012.11.032

[4] Friedman, M.Y., Lenz, E.: The effect of thermal conductivity of tool material on cutting forces and crater wear rate. Wear **25**(1), 39–44 (1973). https://doi.org/10.1016/0043-1648(73)90118-X

[5] Sekulić, M., Jurković, Z., Hadžistević, M., Gostimirović, M.: The influence of mechanical properties of workpiece material on the main cutting force in face milling. Metalurgija **49**(4), 339–342 (2010). Publisher: Hrvatsko Metalursko Društvo (HMD)

[6] Albert, G., Laheurte, R., K'Nevez, J.-Y., Darnis, P., Cahuc, O.: Experimental milling moment model in orthogonal cutting condition: to an accurate energy balance. Int J Adv Manuf Technol **55**(9), 843–854 (2011). https://doi.org/10.1007/s00170-010-3118-0

[7] Royer, R., Cahuc, O., Gerard, A.: Strain Gradient Plasticity Applied to Material Cutting. Advanced Materials Research **423**, 103–115 (2012). https://doi.org/10.4028/www.scientific.net/AMR.423.103. Conference Name: Innovating Processes ISBN: 9783037853290 Publisher: Trans Tech Publications Ltd

[8] Yousfi, W., Cahuc, O., Laheurte, R., Darnis, P., Calamaz, M.: 3D modelling of the mechanical actions of cutting: application to milling. In: Eynard, B., Nigrelli, V., Oliveri, S.M., Peris-Fajarnes, G., Rizzuti, S. (eds.) Advances on Mechanics, Design Engineering and Manufacturing : Proceedings of the International Joint Conference on Mechanics, Design Engineering & Advanced Manufacturing (JCM 2016), 14-16 September, 2016, Catania, Italy. Lecture Notes in Mechanical Engineering, pp. 647–654. Springer, Cham (2017). https://doi.org/10.1007/978-3-319-45781-9_65

[9] San-Juan, M., Martín, O., Santos, F.: Experimental study of friction from cutting forces in orthogonal milling. International Journal of Machine Tools and Manufacture **50**(7), 591–600 (2010). https://doi.org/10.1016/j.ijmachtools.2010.03.013

[10] Yousfi, W., Laheurte, R., Calamaz, M., Darnis, P., Cahuc, O.: 3d kinematic fields studies in milling. Proceedings in Manufacturing Systems **3**(9), 163–168 (2014)

[11] Albert, G.: Identification et modélisation du torseur des actions de coupe en fraisage. These de doctorat, Bordeaux 1 (December 2010). https://www.theses.fr/2010BOR14152

[12] Martelloti, M.E.: An analysis of the milling process. Transactions of the A.S.M.E. **63**(8), 677–700 (1941)